Hindawi
International Journal of Energy Research
Volume 2024, Article ID 8896497, 13 pages
https://doi.org/10.1155/2024/8896497

Research Article

Spatial-Arrangement-Assisted Emission Energy Fine Tuning of CdSe Quantum Dots (QDs) in QD–Block Copolymer Complexes

Jong Dae Jang,[1,2] Hyuk-Jin Seo,[3] Young-Jin Yoon,[3] Young Soo Han,[1] Eun-Joo Shin,[1] and Tae-Hwan Kim[2,3,4,5,6]

[1]*Neutron Science Division, Korea Atomic Energy Research Institute, 111 Daedeok–daero, 989 Beon–gil, Yuseong–gu, Daejeon 34057, Republic of Korea*
[2]*Research Center for Advanced Nuclear Interdisciplinary Technology, Jeonbuk National University, 567 Baekje–daero, Deokjin–gu, Jeonju, Jeollabuk–do 54896, Republic of Korea*
[3]*Department of Applied Plasma & Quantum Beam Engineering, Jeonbuk National University, 567 Baekje–daero, Deokjin–gu, Jeonju, Jeollabuk–do 54896, Republic of Korea*
[4]*High–Enthalpy Plasma Research Center, Jeonbuk National University, 546 Bongdong–ro, Bongdong–eup, Wanju–gun, Jeollabuk–do 55317, Republic of Korea*
[5]*Department of Quantum System Engineering, Jeonbuk National University, 546 Bongdong–ro, Bongdong–eup, Wanju–gun, Jeollabuk–do 55317, Republic of Korea*
[6]*Department of JBNU-KIST Industry-Academia Convergence Research, Jeonbuk National University, Jeonju, Jeollabuk–do 54896, Republic of Korea*

Correspondence should be addressed to Tae-Hwan Kim; taehwan@jbnu.ac.kr

Received 17 October 2023; Revised 24 November 2023; Accepted 15 December 2023; Published 9 January 2024

Academic Editor: Arun Thirumurugan

Quantum dots (QDs) exhibit size-dependent optical properties, where both the absorption and fluorescence energy levels vary with QD size. However, this dependence results in a discontinuity of intrinsically accessible energy levels for the bandgap, posing challenges in achieving precise energy tuning within a specific range. Herein, we demonstrate emission energy control of QDs with identical absorption energy levels by manipulating the spatial arrangement of QDs within QD–polymer complexes through hydrophobic interactions. The phase behavior of the QD–polymer complexes was modulated by adjusting the mass fraction of hydrophilic and hydrophobic blocks in the block copolymer, utilizing two types of amphiphilic block copolymers and varying temperatures. The QDs were spontaneously trapped within the hydrophobic region of the polymer template in water, resulting in spherical, cylindrical, and vesicle structures of QD–polymer complexes, corresponding to spherical, cylindrical, and layered assemblies of QDs, respectively. Depending on the QDs' location within the QD–polymer complex, the surface area in contact with water varied, leading to different degrees of oxidation and, consequently, a change in the fluorescence energy level of QDs. This study introduces a novel method to fine tune the emission energy (<15 eV) of QDs by adjusting the polymer form factor without complicated procedures.

1. Introduction

Semiconductor nanocrystals, known as quantum dots (QDs), possess unique and attractive electronic and optical properties [1–4] that are not observed in bulk materials with sizes above the micrometer scale. Consequently, QDs offer various potential applications, including energy reservoirs, electron carriers, light display, and sensorable materials [2–7]. However, the practical application of QDs is hindered by the narrow and discontinuous accessible energy levels for absorption and fluorescence, which strongly influence their optical properties. While the energy level of QDs can be readily controlled by their size during synthesis [8, 9], the maximum synthesizable size of QDs in the solvothermal method is limited to <6 nm, leading to restrictive accessible energy levels [10]. Furthermore, most QDs contain heavy metals, presenting challenges

in safe handling. Therefore, achieving practical and widespread application of QDs requires precise control over their energy levels for absorption and fluorescence, as well as the development of safe handling methods.

Recently, polymers have been utilized to encapsulate the surface of QDs, improving their safety [2, 11–13], leading to the formation of core-shell-type nanoparticles with a QD core and a polymer shell configuration [14, 15]. In the QD core-polymer shell form, QDs and polymers are used as tracers and drug releasers for the drug delivery system, respectively, to improve the drug delivery performance and biocompatibility [16, 17]. However, the range of applications for polymer encapsulation of QDs remains limited due to the narrow and discrete accessible energy levels determined solely by the synthesis method (size control). Generally, the absorption and emission wavelengths of QDs can be shifted by adjusting their size, but achieving detailed control within specific wavelength ranges has been challenging.

To overcome these limitations, this study proposes utilizing block copolymer phase behavior [15, 18, 19] to achieve a wide range of bandgaps for QDs. With their diverse phase behavior, block copolymers have been employed as templated materials to obtain various nanostructures. When QDs are mixed with block copolymers in an aqueous solution, a complex with diverse nanostructures is expected to form. The spatial arrangement of QDs within the complex can be influenced by interactions between the polymers and QDs, leading to variations in the water contact area of the QDs within the QD–polymer complex. Since the water contact of QDs directly influences their oxidation, controlling the water contact area allows for the modulation of QD oxidation levels. Considering that the fluorescence energy level (emission energy) of QDs depends on their degree of oxidation [18], it was hypothesized that the optical properties of QDs can be controlled through the spatial arrangement of QDs within the QD–polymer complex in an aqueous solution.

To demonstrate the control of emission energy through the QD–polymer complex, CdSe, a typical QD, was chosen as the model system. The CdSe QD was initially prepared in an organic solvent and then mixed with amphiphilic block copolymers in water through emulsification, forming QD–polymer complexes upon evaporation of the organic solvent. For this purpose, amphiphilic block copolymers, specifically poly(ethylene oxide)–poly(allyl glycidyl ether) ($P(EO_x–b–AGE_y)$) diblock copolymers with different values of x and y, were synthesized using living anionic ring-opening polymerization (LAROP) [19]. By mixing two types of $P(EO_x–b–AGE_y)$ block copolymers with different geometrical shapes [20, 21], the phase behavior of the block copolymer was controlled, leading to the formation of QD–polymer complexes with distinct structures.

The morphologies of the CdSe QD–$P(EO_x–b–AGE_y)$ polymer complexes were characterized using small-angle neutron scattering (SANS), revealing spherical, cylindrical, and vesicular structures depending on the mixing ratio of the two types of block copolymers with different geometrical shapes. The different geometrical shapes of the block copolymers resulted in varying curvatures during micellization, thereby influencing the arrangement of QDs within the QD–polymer complex and leading to different water contact areas for the QDs in water. The energy levels (optical properties) of the CdSe QD–$P(EO_x–b–AGE_y)$ polymer complexes with different overall structures were confirmed through ultraviolet–visible (UV–vis) absorbance and photoluminescence (PL) measurements. This validation demonstrated distinct emission energy without changes in the absorption energy of QDs, corresponding to the arrangement of QDs in various geometric phases of the QD–polymer complex.

To the best of our knowledge, this study is the first to demonstrate fine control of the emission energy of QDs through the molecular self-assembly of QD–polymer complexes. This method offers a wide range of energy adjustments for QDs without size limitations, opening up possibilities for various applications. Furthermore, this approach provides new insights into the spatial arrangement of QDs within the polymer matrix.

2. Materials and Methods

2.1. Materials. Several molecules and solvents were prepared to synthesize block copolymers. Poly(ethylene oxide) methyl ether polymer (mPEO; number average molecular weight, Mn = 2000 and 750 g/mol), a monomer of allyl glycidyl ether (AGE; weight average molecular weight, Mw = 114.144 g/mol), potassium cube (in mineral oil), naphthalene (99%), 2.0 M butyl magnesium chloride (in tetrahydrofuran (THF)) solution, 1.4 M sec–butyllithium (in cyclohexane) solution, and anhydrous hexane (99%) were purchased from Sigma-Aldrich (USA). Tetrahydrofuran (THF) was obtained from Junsei (Tokyo, Japan). Anhydrous methanol (99.9%) was purchased from Alfa Aesar (USA). THF and AGE were purified before use. For the synthesis of CdSe QD nanoparticles, cadmium oxide (CdO, 99.5%), oleic acid (90%), selenium (Se, 99.5%), 1–octadecene (90%), and trioctylphosphine (97%) were purchased from Sigma-Aldrich. Solvents ethanol (95%) and N–hexane (95%) were purchased from Samchun Chemical, Inc. (Republic of Korea).

2.2. Purification of AGE and THF. The AGE monomer was purified using 2.0 M butyl magnesium chloride for 30 min and degassed by three freeze-pump-thaw cycles under vacuum. To remove impurities in THF, a mixture of THF and 1.4 M sec–butyllithium was vigorously stirred for 30 min, followed by three cycles of freeze-pump-thaw.

2.3. Synthesis of Block Copolymers. Diblock copolymers of $P(EO_x–b–AGE_y)$ were synthesized via LAROP. The LAROP process is extremely sensitive to oxygen and humidity; therefore, all of the experimental processes were conducted under a vacuum. mPEO polymer blocks with weights of 5 and 1 g (for $P(EO_{46}–b–AGE_{22})$ and $P(EO_{16}–b–AGE_{18})$, respectively) were purified in a vacuum reactor at 45°C and continuously stirred. Then, approximately 5 mL of 0.4 M potassium naphthalenide solution (initiator) was injected into the vacuum reactor, followed by the direct injection of 10 mL of purified THF. After the initiator was injected, the mPEO solution turned dark green, and the initiation reaction

proceeded for 30 min. Subsequently, AGE monomers weighing 5 and 20 g were added to the mPEO polymer solutions for P(EO_{46}–*b*–AGE_{22}) and P(EO_{16}–*b*–AGE_{18}), respectively. The reaction of this mixture was propagated for 20 h, after which the solution turned light brown. The reaction was terminated using anhydrous methyl alcohol. The final solutions were precipitated with hexane, and the remaining hexane in the obtained block copolymer was evaporated under a vacuum for a minimum of 1 d.

2.4. Synthesis of Cadmium Selenide Quantum Dots. A three-step process was performed to prepare the 4.5 nm CdSe QD nanoparticles [10]. First, a solution containing 30 mg selenium in 5 mL of octadecene was prepared in a vial under a nitrogen atmosphere, and 0.4 mL of trioctylphosphine (TOP) was injected into the vial using a syringe (Se/TOP precursor). The Se/TOP precursor was stirred vigorously at 40°C. Second, 19.5 mg of CdO, 0.75 mL of oleic acid, and 15 mL of octadecene were mixed in a round flask under an argon atmosphere (Cd precursor), and the Cd precursor was mixed at 250 rpm as the temperature was increased to 225°C for 45 min. When the temperature of the Cd precursor reached 225°C, 1.5 mL of the Se/TOP precursor was injected into the Cd precursor using a syringe. After 15 min, the CdSe in the octadecene mixture was rapidly cooled using air or water. The cooled mixture was replenished with 120 mL of ethanol. The diluted mixture was centrifuged at 3000 rpm for 10 min, and the quenched CdSe QD nanoparticles were redispersed in hexane (24 mL).

2.5. Preparation of the CdSe–Polymer Mixtures. The samples were prepared by mixing two types of P(EO_x–*b*–AGE_y) diblock copolymers with Mn of 2 K–2.56 K (P(EO_{46}–*b*–AGE_{22})) and 0.75 K–2.05 K (P(EO_{16}–*b*–AGE_{18})) in D_2O. The samples were diluted to facilitate the observation of the micellar shapes. Dilute systems are preferred for observing the formation of molecules in a system because of the absence of interparticle interference. The concentrations of the 2 K–2.56 K samples were fixed to 0.1 wt%, while those of the 0.75 K–2.05 K samples were gradually increased in 0.1 wt% intervals (0, 0.1, 0.2, 0.3, 0.4, and 0.5 wt%) to control the hydrophobicity of the mixtures in 4 mL of D_2O. The prepared polymer mixtures were then divided into two groups. One group was mixed with CdSe QD hexane solution (5 g/L). The CdSe QD hexane solution (0.4 mL) was mixed with the one-polymer mixture group (6 prepared in 2 mL D_2O; hexane was desolvated and dispersed in D_2O by sonication for 8 h). Here, the 2 K–2.56 K (P(EO_{46}–*b*–AGE_{22})) and 0.75 K–2.05 K (P(EO_{16}–*b*–AGE_{18})) block copolymers were labeled as P(46–22) and P(16–18), respectively, for convenience.

2.6. Dynamic Light-Scattering (DLS) Measurements. DLS measurements were conducted using a particle size analyzer (λ = 659 nm, ZetaPLUS, Brookhaven Instruments Corporation, USA) to determine the temperature dependence of the micellar hydrodynamic radius (R_h). The DLS–measured intensity autocorrelation function was obtained using the cumulative method. The normalized values indicate the relative width of the distribution. The corresponding value of R_h was calculated using the Stokes–Einstein equation.

2.7. Small-Angle Neutron-Scattering (SANS) Measurements. SANS measurements were performed using a 40 m SANS at HANARO, Republic of Korea [22]. The configurations were set to cover the Q range of $0.0012\ \text{Å}^{-1} < Q < 0.5\ \text{Å}^{-1}$ for polymer complexes and $0.001\ \text{Å}^{-1} < Q < 0.44\ \text{Å}^{-1}$ for QD–polymer complexes (where $Q = (4\pi/\lambda)\sin(\theta/2)$ is the magnitude of the scattering vector, and θ is the scattering angle). The scattering intensities measured under two different SANS configurations (high- and low-Q regions) were overlapped to cover the entire Q range. All SANS measurements were performed in D_2O to increase neutron-scattering contrast.

2.8. Small-Angle X-Ray-Scattering (SAXS) Measurements. SAXS measurements were performed to obtain Fourier transforms of the hybrid nanostructures. To cover the Q range of $0.012–0.45\ \text{Å}^{-1}$ for polymer complexes and $0.0037–0.6\ \text{Å}^{-1}$ for QD–polymer complexes, the sample–to–detector distance was set to 2 m. The experiments were performed at the 4C and 9A SAXS beamlines of the Pohang Accelerator Laboratory (POSTECH, Republic of Korea) and the NANOPIX laboratory-scale X-ray scattering instrument at the Research Center for Advanced Nuclear Interdisciplinary Technology (JBNU, Republic of Korea).

2.9. Transmission Electron Microscopy (TEM) Observations. A TEM grid was pretreated by glow discharge, after which a sample drop (20 μL) was placed on the grid using a pipette. The sample-containing TEM grid was freeze-dried using liquid nitrogen and a freeze dryer to fix the nanostructures in the studied mixtures. The samples were imaged using corrected (JEM–ARM200F, JEOL, USA) and high-resolution (JEM–2010, JEOL, USA) TEM instruments located at the Jeonbuk National University (Republic of Korea).

2.10. Ultraviolet–Visible Measurements. UV–vis characterization was performed using a UV–vis spectrophotometer (LAMBDA 950, PerkinElmer, Inc., USA). Absorbance was measured in the wavelength range of 190–3000 nm using quartz cuvettes with a 10 mm path length (in this paper, the results for the critical wavelength range of 450–700 nm are presented).

2.11. Photoluminescence (PL) Measurements. PL measurements were performed using a luminescence spectroscope (LS–55, PerkinElmer, Inc., USA). An excitation wavelength of 574 nm was used to measure the emission wavelength of the samples. Emission was measured in the wavelength range of 200–800 nm using quartz cuvettes with a 10 mm path length (in this study, the results for the critical wavelength range of 450–700 nm are presented).

3. Results and Discussions

Although CdSe QDs exhibit different energy levels based on their particle size, there is a limitation to the extent of energy control achievable through particle size manipulation, which

consequently restricts their range of practical applications. Moreover, this energy selectivity linked to particle size results in disparate energy bands, posing challenges in achieving precise energy tuning within specific energy ranges. Therefore, alternative approaches are required to achieve fine adjustments in the energy levels of QDs. Because it is well-known that the spatial arrangement of QDs is highly related to the optical property arising from the interaction of QD, it needs to control it for precise tuning of the energy level of QDs. For this purpose, we used two types of amphiphilic diblock copolymers, P(EO_x–*b*–AGE_y) diblock copolymers, consisting of hydrophilic PEO and hydrophobic PAGE blocks, which were synthesized by LAROP (Figure S1, Supporting Information), as a template to form block copolymer-QD complexes. Herein, the hydrophilic and hydrophobic blocks of the diblock copolymers were varied to induce the rich polymer phase behavior for achieving various spatial arrangements of QDs in the polymer matrix, where the used P(EO_x–*b*–AGE_y) diblock copolymers are P(EO_{46}–*b*–AGE_{22}) and P(EO_{16}–*b*–AGE_{18}) block copolymers (labeled as P(46–22) and P(16–18), respectively), which is characterized by nuclear magnetic resonance (NMR) and gel permeation chromatography (GPC) (Figure S2, Supporting Information). Based on the NMR and GPC measurement results, the Mw (Mw/Mn) of the P(46–22) and P(16–18) block copolymers were calculated to be 2 K–2.56 K (1.04) and 0.75 K–2.05 K (1.13), respectively.

In fact, owing to the energy difference between the emission and absorption of light, the Stokes shift phenomenon in the QDs occurs, presenting a specific color that depends on the QD size. In case of CdSe QDs with different diameters, we confirmed the difference in the Stokes shift by analyzing the absorbance (absorption) and the emission of UV-vis light (Figure S3, Supporting Information), which is similar to the previous studies [8, 9]. Although CdSe QDs have a different energy level per particle size that can be used in various applications, the achievable energy level is still narrow because the size control of QD is limited in the synthesis process. In addition, this energy selectivity with the particle size leads to a discrepancy in the energy bands, making it challenging to achieve precise energy tuning within a specific energy range. To achieve a broad spectrum of the energy level of CdSe QDs, therefore, CdSe QDs with a representative size (4.5 nm, which has the lowest Stokes shift) were used, and then, their emission energies were systematically investigated in the P(EO_x–*b*–AGE_y) diblock copolymer matrix. Herein, the sizes of the CdSe QDs (4.5 nm with the particle size distribution of 0.07) were characterized by small-angle X-ray-scattering (SAXS) and transmission electron microscopy (TEM) measurements (Figure S4, Supporting Information). The surface of the CdSe QDs was functionalized with hydrophobic oleic acid molecules, which are insoluble in aqueous solutions. To form a complex structure of QDs–P(*X*–*Y*), two types of block copolymers and a CdSe QD (4.5 nm particle size) solution were mixed. Amphiphilic block copolymers in aqueous solutions enhance the solubility of materials with one-sided properties, such as hydrophobic CdSe QDs, forming a collective oil-in-water microemulsion of CdSe QDs and block copolymer blends. During sonication for 8 h, the CdSe nanoparticles were stably localized in the interior of the block copolymer aggregate upon hydrophobic interaction. Therefore, the CdSe QD–P(*X*–*Y*) polymer complexes were well-dispersed in the aqueous solution despite the large hydrophobic volume (Figure 1).

Since CdSe QDs can also incorporate into specific hydrophobic regions of the block copolymer upon the hydrophobic interactions, the microstructure of QD-block copolymer complexes can be transformed into other structures such as spherical, cylindrical, and vesicular nanostructures based on the volume fraction (ϕ) of the hydrophilic and hydrophobic blocks of the polymer when compared to the original micellar phase of the block copolymer only. DLS measurements were performed to determine the micelle size distributions of the complexes. The P(46–22)/P(16–18) complex formed small particles of approximately 20 nm in size (Figure 1(d)), which are expected to be spherical micelles of the general core–shell sphere nanoparticle size. However, when CdSe QDs were added to the polymer complex, the CdSe QD–P(46–22)/P(16–18) polymer complexes exhibited large structures of approximately 120–180 nm, which is not the general size of the core-shell spherical structure. Since a specificity was found in the DLS measurement, SANS measurements were performed to investigate the detailed shapes of the CdSe QD–P(46–22)/P(16–18) polymer complex structure (Figure 2).

Figures 2(a) and 2(b) show the SANS intensities of the P(46–22)/P(16–18) polymer solutions and CdSe QD–P(46–22)/P(16–18) polymer complexes. When only the P(46–22)/P(16–18) polymer was present in the solution, the SANS intensities exhibited q^0 behavior, and a sphere with a core–shell form factor model successfully reproduced the SANS intensities (Figure 2(a)). These findings suggest that the polymer mixtures formed general spherical structures in the solution. However, after the CdSe QDs were added, the slopes of the SANS intensities changed to approximately q^{-2} or q^{-1}, depending on the structural transformation (Figure 2(b)) [23, 24]. At a P(16–18) polymer concentration of 0.0%, the SANS intensity exhibited q^{-2} behavior; however, the trend of the intensity graph shape shows the cylindrical structure. The slightly strange shape of the P(16–18) polymer concentration of 0.0% suggested a typical mixed phase in the solution. As the P(16–18) polymer concentration increased, the volumetric fraction of vesicular structures increased, thereby decreasing the hydrophilic volume in the complex structure [25]. To confirm the nanostructure of the CdSe QD–P(46–22)/P(16–18) polymer complexes, the SANS intensities were successfully reproduced using summed form factor models (Figures 2(b) and 2(d)). The model parameters of the P(46–22)/P(16–18) polymer solutions and CdSe QD–P(46–22)/P(16–18) polymer complexes were calculated as shown in Figures 2(c) and 2(d), and the structural volumetric fraction was calculated as shown in Figure 2(e). The nanostructures of the P(46–22)/P(16–18) polymer complexes were found to have small sizes of ~20 nm, while the nanostructures of the CdSe QD–P(46–22)/P(16–18) polymer complexes exhibited larger sizes of ~130 nm. The results obtained from the SANS particle size analyses were consistent with those of the DLS

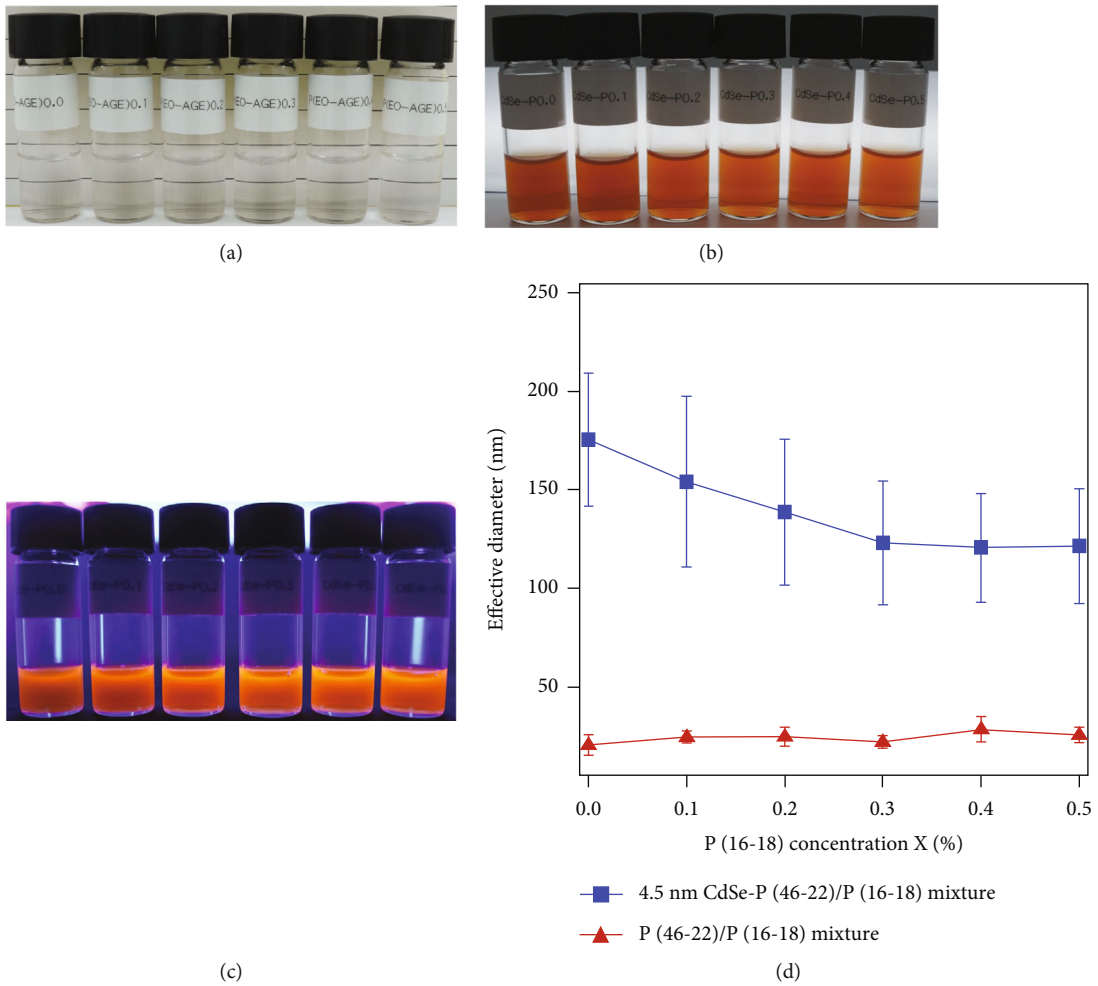

Figure 1: Photos of solutions and dynamic light-scattering results of the complexes. Photos of the (a) P(46–22)/P(16–18) solution, (b) CdSe QDs–P(46–22)/P(16–18) polymer solution under visible light, and (c) CdSe QDs–P(46–22)/P(16–18) polymer solution under UV light. (d) Dynamic light-scattering results of the P(46–22)/P(16–18) and CdSe QDs–P(46–22)/P(16–18) polymer solutions.

measurements. For further details of the SANS analysis results, the detailed parameters of the complex vesicle structure were calculated and presented in Table S1. Based on the SANS detailed analysis, the vesicle size was determined to be 80 ± 2 nm, and the vesicles contained approximately 100–180 QDs. To confirm the appearance of the CdSe QD–P(46–22)/P(16–18) polymer complexes, TEM measurements were performed to confirm the structural distributions (Figure 3).

According to the TEM measurement results, the CdSe QD–P(46–22) 0.1%/P(16–18) 0.1% and 0.2% complexes exhibited a mixed phase consisting of cylindrical and vesicular structures in the images. Specifically, the CdSe QD–P(46–22) 0.1%/P(16–18) 0.1% sample displayed a mixed phase where the cylindrical structure predominated (Figure 3(b)). Despite the QDs' images appearing scattered, the observed contrast indicated the presence of cylindrical structures (red dotted lines). On the other hand, in the CdSe QD–P(46–22) 0.1%/P(16–18) 0.2% sample, although the mixed phase contained cylindrical and vesicular structures, the cylindrical structures were relatively less pronounced compared to those observed in the TEM image of the CdSe QD–P(46–22) 0.1%/P(16–18) 0.1% sample (Figure 3(c)). It is important to note that the TEM images of the CdSe QD–P(46–22) 0.1%/P(16–18) 0.1% and 0.2% samples exhibited the formation of vesicular structures, which differed from the typical core-shell sphere structure. These observations are consistent with the SANS analyses, further corroborating the evidence that the CdSe QD–P(46–22)/P(16–18) polymer complexes adopt a mixed phase composed of cylindrical structures hundreds of nanometers in length and large vesicular structures measuring approximately 100 nm in size.

The optical properties of the CdSe QD–P(46–22)/P(16–18) polymer complexes can be affected by their overall structures, which are influenced by changing the polymer structure conformation that leads to a different spatial arrangement of QDs in the complex. The light absorption and emission properties of the CdSe QD–P(46–22)/P(16–18) polymer complexes were characterized by using UV–vis and PL measurements, respectively (Figure S5). In contrast to those of the CdSe QD solution, the absorption wavelengths of the CdSe QD–P(46–22)/P(16–18) polymer complexes did not shift to other wavelengths, as shown in the light absorption graphs (Figure S5a). This indicates that the intrinsic properties of CdSe QDs are not altered by forming a polymer shell on the

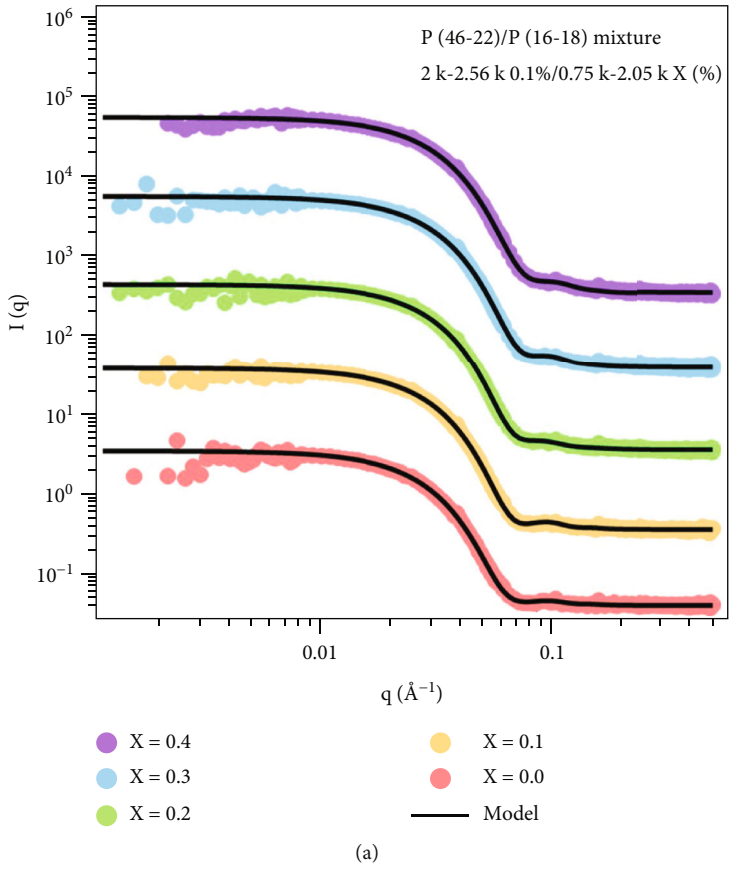

(a)

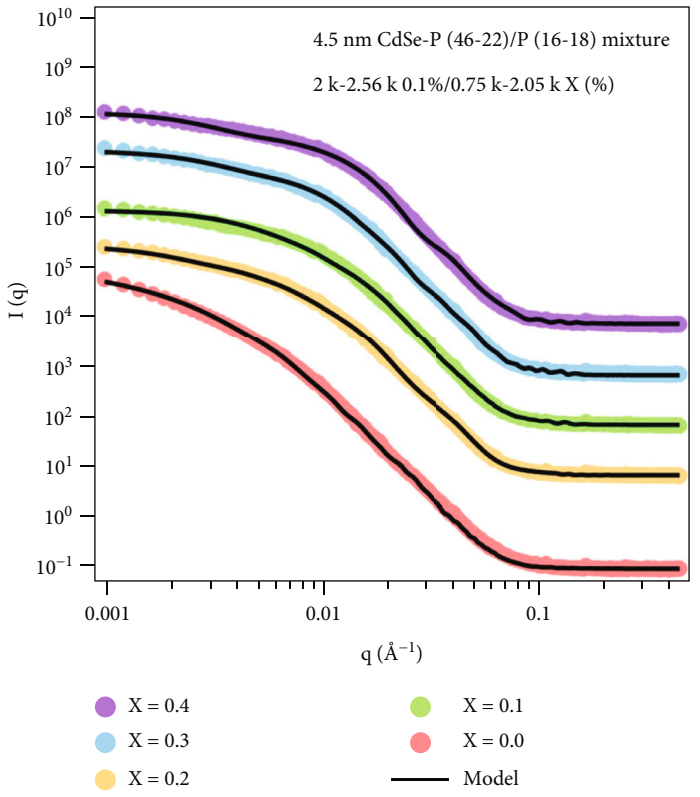

(b)

Figure 2: Continued.

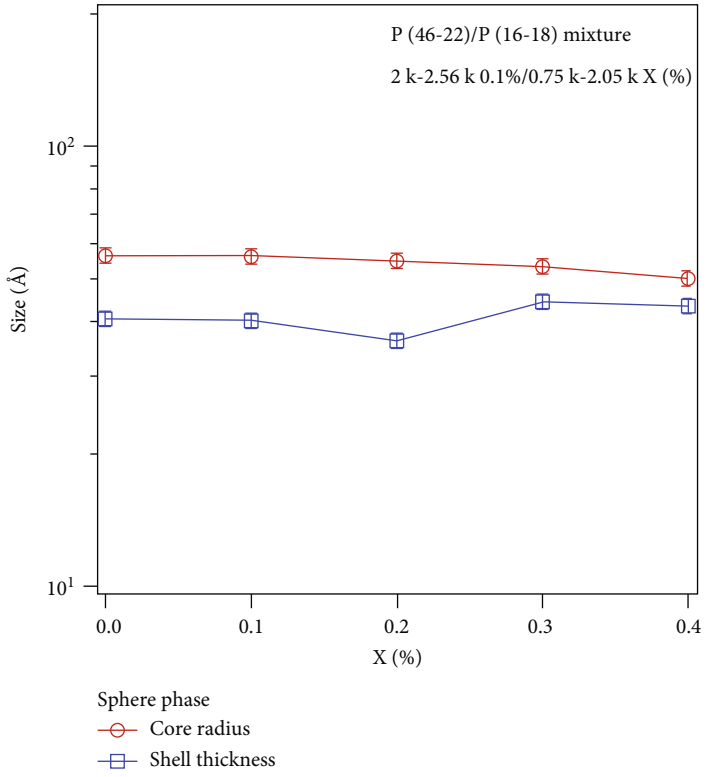

(c)

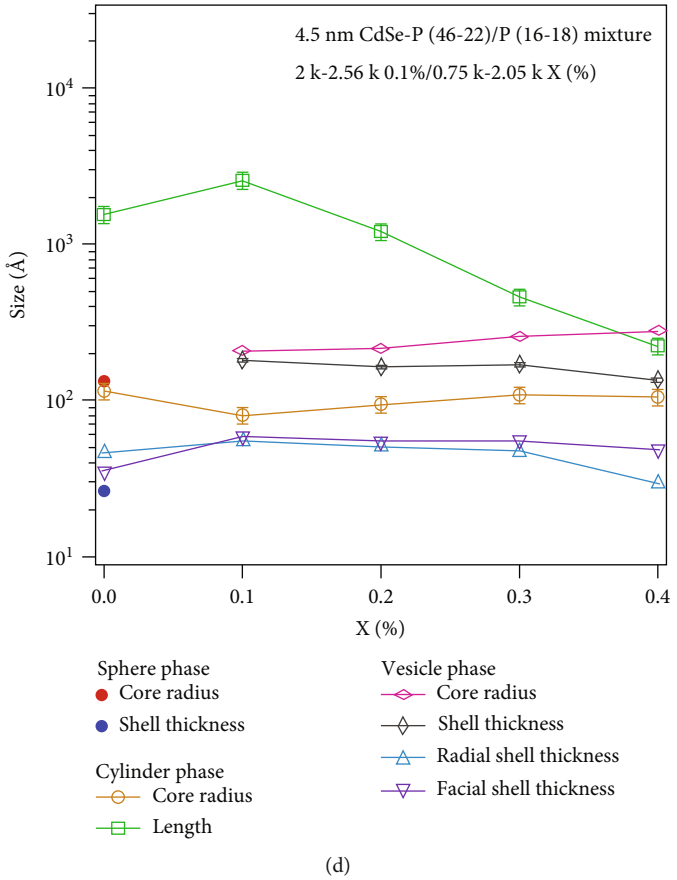

(d)

Figure 2: Continued.

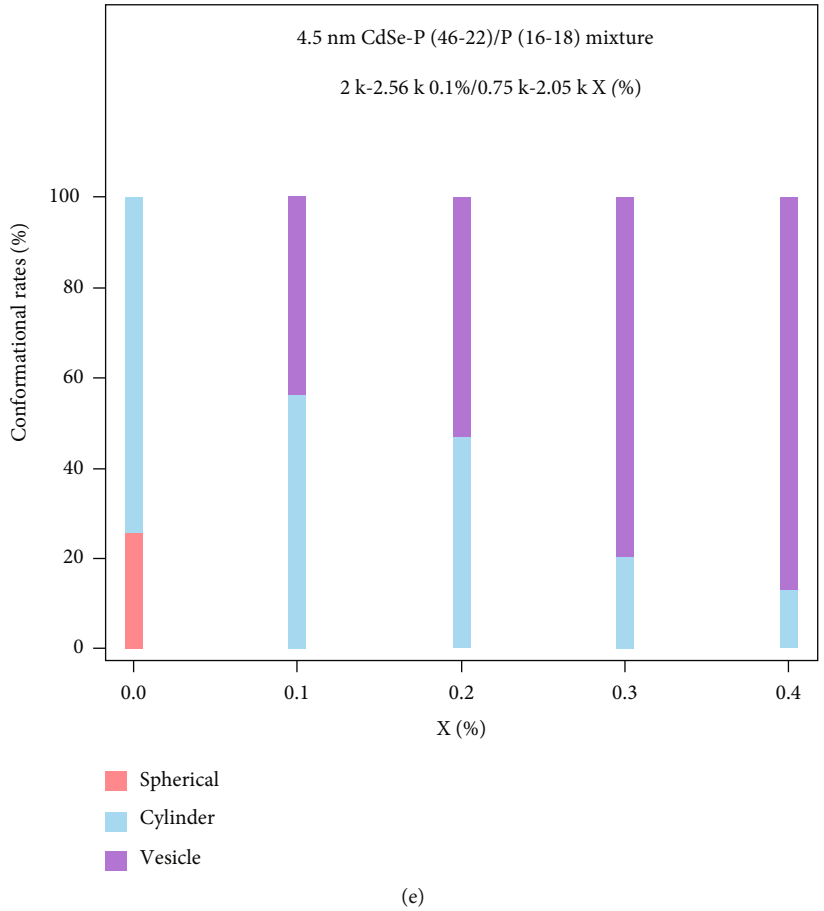

Figure 2: SANS intensities of the P(46–22)/P(16–18) polymer solution and CdSe QDs–P(46–22)/P(16–18) polymer complexes at 25°C. (a, b) The results of the SANS intensities with the form factor model shown. (c, d) The parameters of the form factors. (e) The volumetric fractions of the complex nanostructures in the solutions.

CdSe QD surface [20, 21, 26], suggesting that the CdSe QDs do not aggregate to form large particles in the mixture. However, the light emission wavelengths changed depending on the P(16–18) polymer concentration (Figure S5b); the CdSe QD–P(46–22)/P(16–18) polymer solutions exhibited different light emission wavelengths. In particular, the emission wavelengths of CdSe QDs at concentrations of P(46–22) 0.1%/P(16–18) 0.1% and 0.2% polymer complexes and at concentrations of P(46–22) 0.1%/P(16–18) 0.0%, 0.3%, 0.4%, and 0.5% polymer complexes varied, shifting to 593, 588.5, 588, and 586 nm, respectively. Then, the structural characteristics of the CdSe QD–P(46–22)/P(16–18) polymer complexes, which are confirmed by the SANS analysis, depends on the emission wavelength shift [27]. This phenomenon can occur due to the way the polymer molecules interact with CdSe QDs, thus altering their electronic properties.

The differences in light absorption and emission for each CdSe QD–P(46–22)/P(16–18) polymer complex are shown in Figure 4(a). The Stokes shift and energy levels of the CdSe QD–P(46–22)/P(16–18) polymer complexes were then converted from light absorption and emission wavelengths to wavenumbers (Figure 4(b)). Figure 4(a) shows that the emission wavelengths of the CdSe QD–P(46–22)/P(16–18) polymer complex shifted to a lower wavelength than those of the CdSe QD solution. This shift can be attributed to the formation of a polymer shell around the CdSe QDs [2, 8], which is expected to cause a blue shift. The degree of the blue shift was calculated using the Doppler effect (Figure 4(b)), where $z = (\lambda_{abs.} - \lambda_{emit.})/\lambda_{emit.}$ [28]. By calculating the degree of the blue shift, the energy-level changes in response to changes in light emission can be evaluated. The energy level was also calculated based on the degree of blue shift; evidently, the blue shift phenomenon was stronger for the sphere-shaped structure than for the cylinder-shaped structure (Figures 2(e) and 4(b)). Furthermore, the blue shift phenomenon was more pronounced in the CdSe QD–P(46–22)/P(16–18) polymer complexes with P(16–18) polymer concentrations of 0.0%, 0.3%, 0.4%, and 0.5% compared to those with the P(16–18) polymer concentrations of 0.1% and 0.2% (Figure 4(c)). These results indicate that the emission energy level of CdSe QDs can be controlled by altering the structure of the CdSe QD–P(46–22)/P(16–18) polymer complex. The geometrical variations within the CdSe QD–P(46–22)/P(16–18) polymer complex play a pivotal role in inducing phase transitions, leading to distinct degrees of curvature in the resulting nanostructures. The

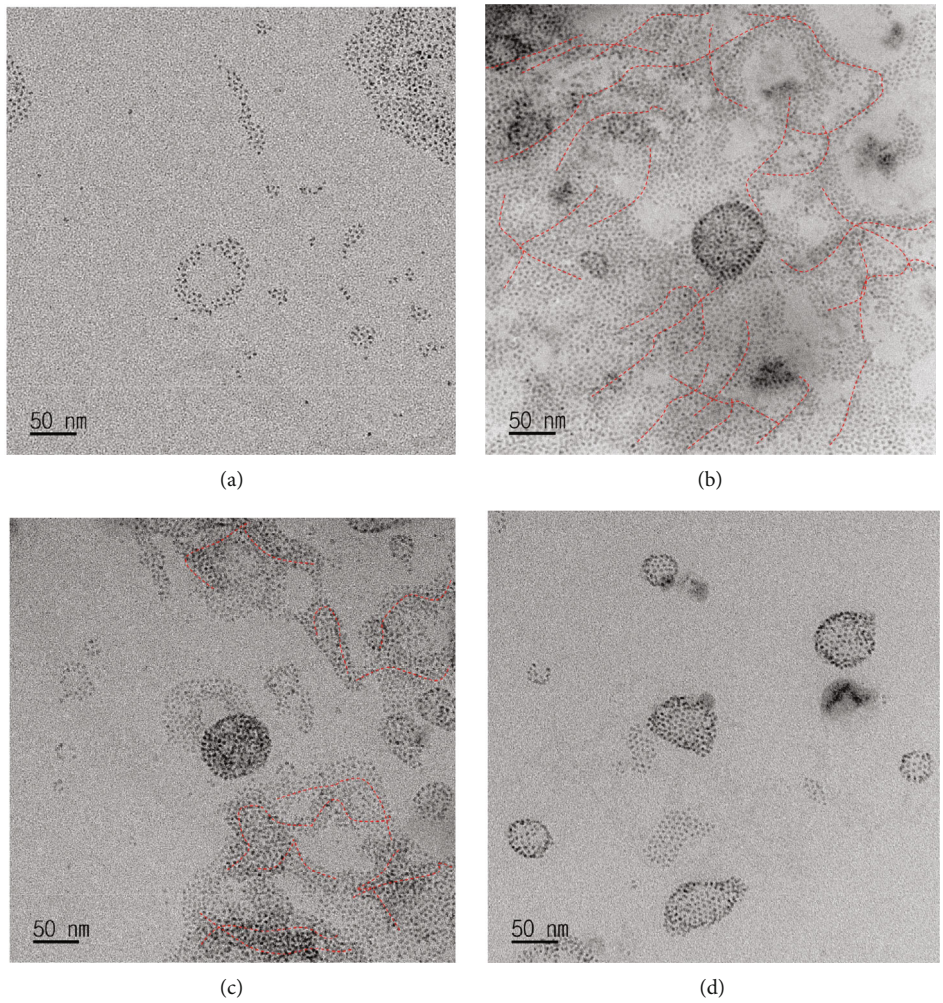

Figure 3: Transmission electron microscopy (TEM) images of the 4.5 nm CdSe QDs–P(46–22)/P(16–18) polymer complexes at 25°C. The complexes of 4.5 nm CdSe–P(46–22) 0.1% with (a) P(16–18) 0.0%, (b) P(16–18) 0.1%, (c) P(16–18) 0.2%, and (d) P(16–18) 0.4%. The red dotted lines indicate the cylindrical structures.

changes in the curvature of the polymer template significantly impact the probability of QDs, existing within the polymer template coming into contact with water molecules outside the template. The cylindrical shapes have a larger curvature rather than the sphere-shaped structure such as the spherical and vesicular shapes. Therefore, the CdSe QD–P(46–22)/P(16–18) polymer complexes of the P(16–18) polymer concentrations of 0.1% and 0.2% had a rather small oxidation compared to the CdSe QD–P(46–22)/P(16–18) polymer complexes with P(16–18) polymer concentrations of 0.0%, 0.3%, 0.4%, and 0.5%. This variation in water contact leads to a modulation in the oxidation degree of CdSe QDs. As the previous studies have indicated, the oxidation degree of QDs strongly influences their fluorescence energy (emission energy), establishing a direct relationship between the oxidation degree and the energy level of the QD–polymer complexes [18]. Herein, QDs underwent the blue shift when they formed the complex nanostructure with the polymers. This can be explained by the adsorption of the ether group of poly(allyl glycidyl ether) (which is a hydrophobic block but with a polarity like the ester group [29]) on the CdSe QD surface due to its slight hydrophilic characteristics. The vacant orbitals and dangling bonds occupied by the electron lone pairs of the ether groups adsorbed on the CdSe QD surface fill the potential conduction–band electron traps and confine the wave function to the CdSe QD core [34–37]. This enhanced confinement induces a blue shift in the PL spectrum of the CdSe QD–P(46–22)/P(16–18) polymer complexes. In addition, the CdSe QD–P(46–22)/P(16–18) polymer complexes with the P(16–18) polymer concentrations of 0.1% and 0.2%, which has a relatively larger curvature, show a rather small blue shift in the PL peaks. The phenomenon occurred via the photocorrosion of the CdSe QD surface because of the dissolved oxygen in the water. In the photocorrosion process, Se becomes to SeO_2, and this oxidation leads the decrease of the CdSe QD size. Since the CdSe QD–P(46–22)/P(16–18) polymer complexes with the P(16–18) polymer concentrations of 0.1% and 0.2% are less oxidized due to relatively little water contact, they have rather a small blue shift than those of 0.0%, 0.3%, 0.4%, and 0.5%.

Based on SANS analyses with the form factor models, the CdSe QD–P(46–22)/P(16–18) polymer complexes formed spherical, cylindrical, and vesicle structures, with the number

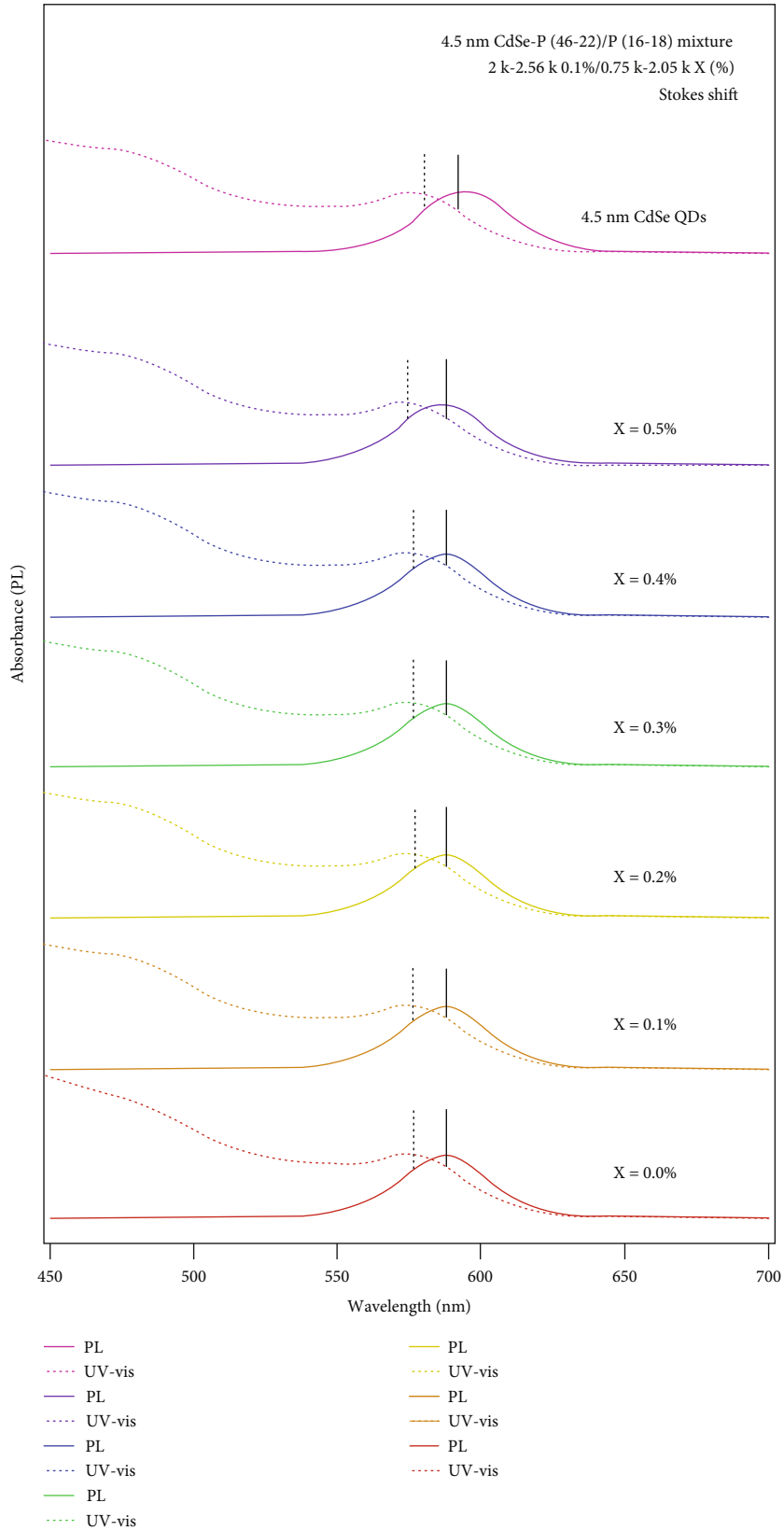

(a)

Figure 4: Continued.

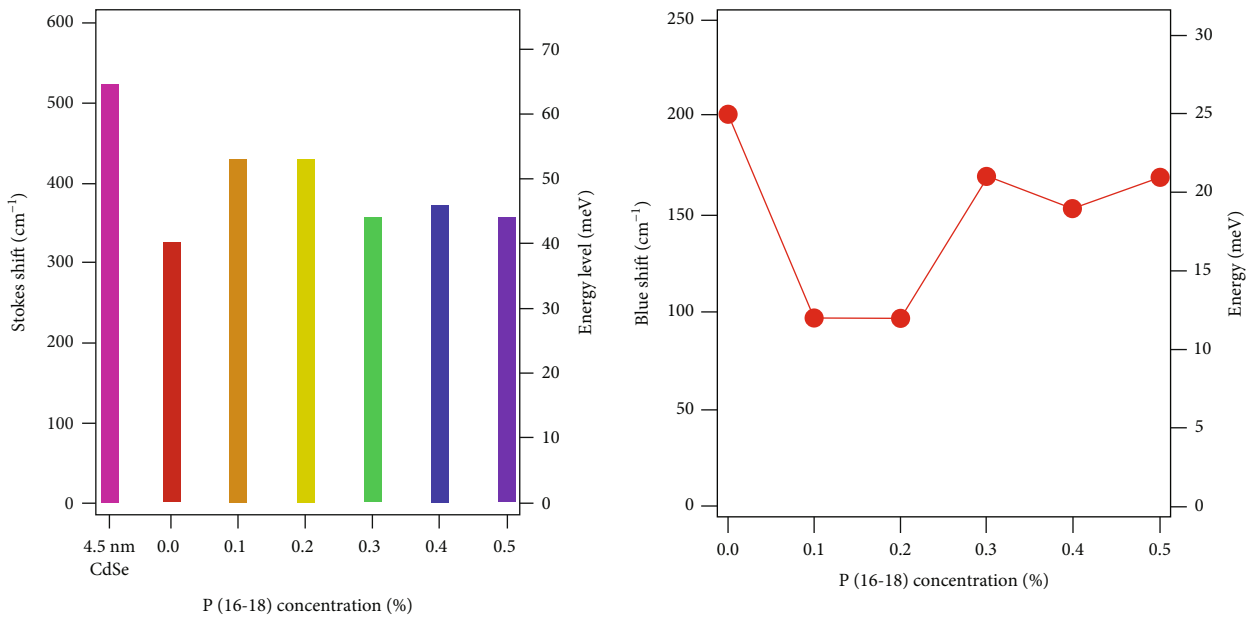

Figure 4: Energy-level evaluations of the CdSe QDs–P(46–22)/P(16–18) polymer complexes. (a) Overlapped data of the UV–vis and PL measurements. Calculation of the (b) Stokes shift degrees and (c) blue shift degrees.

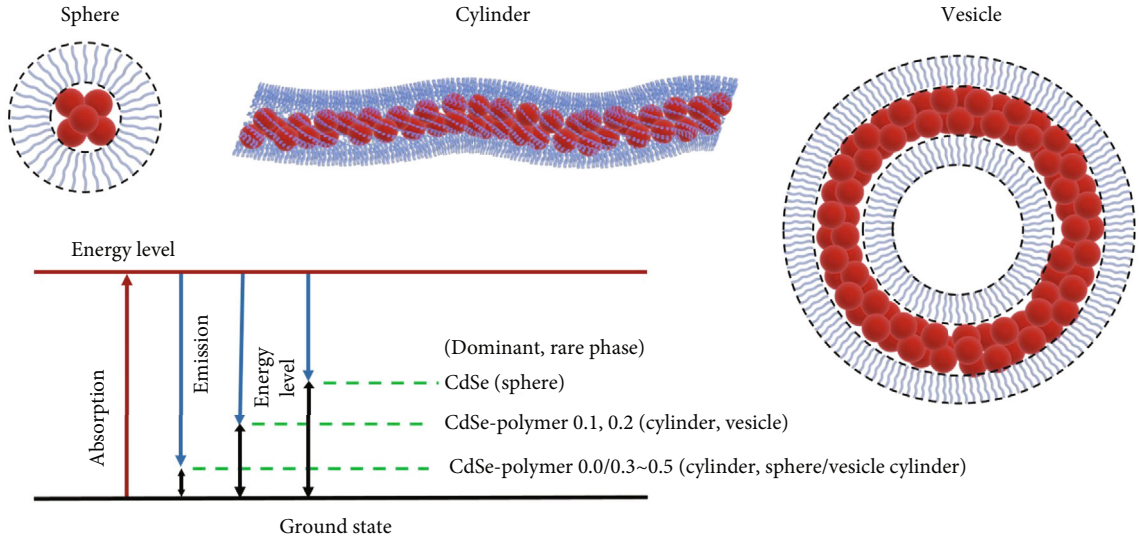

Figure 5: Schematic of the CdSe QDs–P(46–22)/P(16–18) polymer nanostructures and changes in emission energy levels.

of CdSe QDs in the hydrophobic region being approximately 9.6, 111.1, and 1859.2, respectively. Therefore, according to the SANS analyses and absorbance/emission wavelength measurements, the blue shift phenomenon became stronger when the CdSe QD–P(46–22)/P(16–18) complex formed a sphere-shaped structure (spherical and vesicular structures) rather than a cylinder-shaped structure. To better illustrate the changes in the optical properties of the CdSe QD–P(46–22)/P(16–18) polymer complex nanostructures, a simplified schematic is shown in Figure 5. This figure highlights the key conformational differences that lead to the observed variations in the optical spectra.

Overall, in metal–organic complex nanoparticles such as QD–polymers, the change in energy level originates from the localized surface plasmon resonance (LSPR) of the metal, which can be altered by a change in electron dominance, conformation, and size of the metal atoms. However, metal–organic complex nanoparticles possess an interface between the metal and the organic material; thus, electron domination can be changed by the geometrical shape of the organic material. Several methods have been reported for controlling the particle size or LSPR of metal nanoparticles using an inorganic–inorganic complex [8, 9, 30–32]. Studies using organic–inorganic mixed materials have been

conducted; however, these studies have employed a fragmentary form as an inorganic core–organic shell structure [29, 33]; moreover, the LSPR control is limited. The CdSe QD-P(46–22)/P(16–18) polymer complex showed different shapes, and their geometrical changes affected the LSPR of the complex structure. The phase behavior of the CdSe QD–P(46–22)/P(16–18) polymer complex leads to a nanoscale decrease in the interparticle distance of the CdSe QDs, as indicated by the PL intensities; this can be translated into the degrees of their energy levels, with the sphere-shaped structures exhibiting a larger change in the energy level than the cylindrical structures. This result is not limited to a general core–shell spherical structure using a variety of QD–polymer complexes in the core–shell form. However, it indicates a novel solution that transforms ideas using structural conformation changes in the energy-level section of metallic nanoparticles.

4. Conclusion

This study presents a comprehensive investigation of the emission energy transition of QDs within the QD–polymer complexes, which is achieved without causing shifts in the absorption energy. As we observed, the optical properties of QDs themselves are predominantly controlled by their size, with both the absorption and fluorescence energy levels being intricately linked to the QD size. However, this size dependence leads to a challenging discontinuity in the intrinsic energy level for the bandgap, making precise energy tuning within specific energy levels difficult to achieve. To overcome this limitation and achieve fine control over the emission energy, we harnessed the phase behavior of QD–polymer complexes, offering varying spatial distributions of QDs. Using amphiphilic block copolymers with different geometries as templates for QD self-assembly, we obtained QD–polymer complexes with diverse overall structures, including spheres, cylinders, and vesicles, each housing QDs. The SANS, UV–vis absorbance, and PL measurements demonstrated that the overall sphere-shaped structures exhibited smaller energy-level differences compared to the overall cylinder-shaped structures. Notably, when the CdSe QD–P(46–22)/P(16–18) polymer complex formed a cylinder-shaped structure, the curvature was maximal, leading to decreased oxidation of the CdSe QDs. On the other hand, spherical structures featured smaller curvatures, effectively enhancing the probability of CdSe QD oxidation within the QD-polymer complex. As a result, the spherical structures yielded a substantial emission energy shift of approximately 15 eV for the CdSe QDs. The significant findings of this study shed new light on the precise control of optical properties for nanoparticles, emphasizing the critical role of the template's phase behavior in controlling QD arrays and oxidation degrees. By exploiting the versatility of amphiphilic block copolymers as templates, we have demonstrated a promising approach for achieving tailored emission energy levels of QDs within the QD–polymer complexes.

Data Availability

The data that support the findings of this study are available from the corresponding author upon reasonable request.

Conflicts of Interest

The authors declare no conflict of interest.

Authors' Contributions

JDJ was in charge of the conceptualization. JDJ and THK were in charge of the methodology. JDJ and HJS oversaw the investigation. YJY, YSH, EJS, and THK were in charge of the visualization. YSH, EJS, and THK provided supervision. JDJ wrote the original draft. JDJ and THK reviewed and edited the manuscript. Jong Dae Jang and Hyuk–Jin Seo contributed equally to this work.

Acknowledgments

This work was supported by the National Research Foundation of Korea (NRF) and the Commercialization Promotion Agency for R&D Outcomes (COMPA) grant, funded by the Ministry of Science and ICT of Korea (Grant nos. NRF–2020R1I1A3A04036603, NRF–2020K1A3A7A09078089, NRF-2021M2D2A1A02041482, NRF–2017M2A2A6A05017651, and RS-2023-00304743), and the internal R&D program at the Korea Atomic Energy Research Institute (KAERI) funded by the Ministry of Science and ICT of Korea (1711197095 and 1711173802). We thank the Pohang Accelerator Laboratory, the HANARO Center at KAERI, and the Center for University-wide Research Facilities (CURF) at Jeonbuk National University for performing the SAXS, SANS, and TEM experiments, respectively.

Supplementary Materials

Synthesis of the P(EO_x-*b*-AGE_y) block copolymers (PDF). ^{1}H-NMR spectra and GPC traces of the P(EO_x-*b*-AGE_y) diblock copolymers (PDF). Photographs, light absorption and emission, and calculation of Stokes shift and bandgap energy level of CdSe QDs with diameters of 2.9, 3.0, 3.3, and 4.5 nm (PDF). SAXS measurement and TEM image of CdSe QD (PDF). UV–vis and photoluminescence spectra of CdSe-P(EO_x-*b*-AGE_y) mixtures (PDF). The detailed parameters of the complex vesicle structure (PDF). *(Supplementary Materials)*

References

[1] T. Kim, Y. Jung, and J. K. Lee, "The formation mechanism of CdSe QDs through the thermolysis of $Cd(oleate)_2$ and TOPSe in the presence of alkylamine," *Journal of Materials Chemistry C*, vol. 2, no. 28, pp. 5593–5600, 2014.

[2] A. Sabah, S. Tasleem, M. Murtaza, M. Nazir, and F. Rashid, "Effect of polymer capping on photonic multi-core–shell quantum dots CdSe/CdS/ZnS: impact of sunlight and antibacterial activity," *The Journal of Physical Chemistry C*, vol. 124, no. 16, pp. 9009–9020, 2020.

[3] O. Chen, J. Zhao, V. P. Chauhan et al., "Compact high-quality CdSe–CdS core–shell nanocrystals with narrow emission linewidths and suppressed blinking," *Nature Materials*, vol. 12, no. 5, pp. 445–451, 2013.

[4] J. Liu, G. Luo, S. Mi, J. Zheng, and C. Xu, "Trifunctional CdSe quantum dots-polymer composite film with electrochromic, electrofluorescent and light-induced coloration effects," *Solar Energy Materials and Solar Cells*, vol. 177, pp. 82–88, 2018.

[5] Q. Ran, Z. Fan, X. Guo et al., "Simultaneous adsorption and fluorescent detection of Cr(VI) via lanthanide coordinating polymeric porous microparticles," *Chemical Engineering Journal*, vol. 457, article 141214, 2023.

[6] K. Jia, K. Yi, W. Zhang, P. Yan, S. Zhang, and X. Liu, "Carbon nanodots calibrated fluorescent probe of QD@amphiphilic polyurethane for ratiometric detection of Hg (II)," *Sensors and Actuators B: Chemical*, vol. 370, article 132443, 2022.

[7] X. He, K. Jia, Y. Bai et al., "Quantum dots encoded white-emitting polymeric superparticles for simultaneous detection of multiple heavy metal ions," *Journal of Hazardous Materials*, vol. 405, article 124263, 2021.

[8] J. Zhang, S.–. Q. Zhao, K. Zhang, K. J.–. Q. Zhou, and Y.–. F. Cai, "A study of photoluminescence properties and performance improvement of Cd-doped ZnO quantum dots prepared by the sol–gel method," *Nanoscale Research Letters*, vol. 7, no. 1, pp. 1–7, 2012.

[9] W. W. Yu, L. Qu, W. Guo, and X. Peng, "Experimental determination of the extinction coefficient of CdTe, CdSe, and CdS nanocrystals," *Chemistry of Materials*, vol. 15, no. 14, pp. 2854–2860, 2003.

[10] K. J. Nordell, E. M. Boatman, and G. C. Lisensky, "A safer, easier, faster synthesis for CdSe quantum dot nanocrystals," *Journal of Chemical Education*, vol. 82, no. 11, pp. 1697–1699, 2005.

[11] R. E. Anderson and W. C. W. Chan, "Systematic investigation of preparing biocompatible, single, and small ZnS-capped CdSe quantum dots with amphiphilic polymers," *ACS Nano*, vol. 2, no. 7, pp. 1341–1352, 2008.

[12] Q. Zhou, Z. Li, Q. Wang, L. Peng, S. Luo, and F. L. Gu, "Polymer-capped CdSe/ZnS quantum dots for the sensitive detection of Cu^{2+} and Hg^{2+} and the quenching mechanism," *Analytical Methods*, vol. 13, no. 20, pp. 2305–2312, 2021.

[13] A. F. E. Hezinger, J. Teßmar, and A. Göpferich, "Polymer coating of quantum dots – a powerful tool toward diagnostics and sensorics," *European Journal of Pharmaceutics and Biopharmaceutics*, vol. 68, no. 1, pp. 138–152, 2008.

[14] A. Fokina, Y. Lee, J. H. Chang et al., "The Role of Emission Layer Morphology on the Enhanced Performance of Light-Emitting Diodes Based on Quantum Dot-Semiconducting Polymer Hybrids," *Advanced Materials Interfaces*, vol. 3, no. 18, article 1600279, 2016.

[15] L. Dworak, A. Bottin, S. Roth et al., "Photodynamics at the CdSe quantum dot–perylene diimide interface: unraveling the excitation energy and electron transfer pathways," *The Journal of Physical Chemistry C*, vol. 125, no. 6, pp. 3277–3284, 2021.

[16] P. Kumar, M. Patel, C. Park et al., "Highly luminescent biocompatible $CsPbBr_3@SiO_2$ core–shell nanoprobes for bioimaging and drug delivery," *Journal of Materials Chemistry B*, vol. 8, no. 45, pp. 10337–10345, 2020.

[17] M. Patel, R. Patel, C. Park et al., "Water-stable, biocompatible, and highly luminescent perovskite nanocrystals-embedded fiber-based paper for anti-counterfeiting applications," *Nano Convergence*, vol. 10, no. 1, p. 21, 2023.

[18] A. Kitai, *Luminescent Materials and Applications*, Wiley–VCH, New York, 2008.

[19] J. D. Jang, C. Do, J. Bang, Y. S. Han, and T.-H. Kim, "Self-assembly of temperature sensitive unilamellar vesicles by a blend of block copolymers in aqueous solution," *Polymers*, vol. 11, no. 1, pp. 63–73, 2019.

[20] J. D. Jang, M. Bae, C. Do et al., "Self-Assembly of 2D Gold Nanoparticle Superlattice in a Polymer Vesicle Layer Driven by Hydrophobic Interaction," *The Journal of Physical Chemistry Letters*, vol. 12, no. 28, pp. 6736–6743, 2021.

[21] J. D. Jang, H. J. Seo, Y. J. Yoon, S. H. Choi, Y. S. Han, and T. H. Kim, "Conformational control of two-dimensional gold nanoparticle arrays in a confined geometry within a vesicular wall," *Scientific Reports*, vol. 12, no. 1, pp. 4548–4557, 2022.

[22] Y. S. Han, S. M. Choi, T. H. Kim, C. H. Lee, S. J. Cho, and B. S. Seong, "A new 40 m small angle neutron scattering instrument at HANARO, Korea," *Nuclear Instruments and Methods in Physics Research Section A: Accelerators, Spectrometers, Detectors and Associated Equipment*, vol. 721, pp. 17–20, 2013.

[23] B. Hammouda, "SANS from Pluronic P85 in d-water," *European Polymer Journal*, vol. 46, no. 12, pp. 2275–2281, 2010.

[24] J. Lee, V. Agarwal, A. Bose, G. F. Payne, and S. R. Raghavan, "Transition from unilamellar to bilamellar vesicles induced by an amphiphilic biopolymer," *Physical Review Letters*, vol. 96, no. 4, article 048102, 2006.

[25] M. D. Tikekar, K. T. Delaney, M. C. Villet, R. T. Douglas, and H. F. Glenn, "A phase field model for dynamic simulations of reactive blending of polymers," *Soft Matter*, vol. 18, no. 4, pp. 877–893, 2022.

[26] J. D. Jang, S. W. Jeon, Y. J. Yoon, J. Bang, Y. S. Han, and T. H. Kim, "Self-assembly of gold nanoparticles in a block copolymer aggregate template driven by hydrophobic interactions," *Polymer Chemistry*, vol. 10, no. 46, pp. 6269–6277, 2019.

[27] J. R. Gispert, *Coordination Chemistry*, Wiley–VCH, New York, 2008.

[28] J. Rosen and L. Q. Gothard, *Encyclopedia of Physical Science*, Infobase Publishing, New York, 2009.

[29] W. Guo, J. Yuan, H. Yuan et al., "Ultrafast electron transfer in low-band gap polymer/PbS nanocrystalline blend films," *Advanced Functional Materials*, vol. 26, no. 5, pp. 713–721, 2016.

[30] S. Jiao, Q. Shen, I. Mora-Seró et al., "Band engineering in core/shell ZnTe/CdSe for photovoltage and efficiency enhancement in exciplex quantum dot sensitized solar cells," *ACS Nano*, vol. 9, no. 1, pp. 908–915, 2015.

[31] X. Cao, Q. Zhang, C. Zhang et al., "A novel approach to coat silica on quantum dots: forcing decomposition of tetraethyl orthosilicate in toluene at high temperature," *Journal of Alloys and Compounds*, vol. 817, article 152698, 2020.

[32] X. Wang, W. Li, and K. Sun, "Stable efficient CdSe/CdS/ZnS core/multi-shell nanophosphors fabricated through a phosphine-free route for white light-emitting-diodes with high color rendering properties," *Journal of Materials Chemistry*, vol. 21, no. 24, pp. 8558–8565, 2011.

[33] W. N. Wenger, F. S. Bates, and E. S. Aydil, "Functionalization of cadmium selenide quantum dots with poly(ethylene glycol): ligand exchange, surface coverage, and dispersion stability," *Langmuir*, vol. 33, no. 33, pp. 8239–8245, 2017.